A Time-Dependent DFT Study of Copper (II) Oxo Active Sites for Methane-to-Methanol Conversion in Zeolites

Kevin Curtis, Dipak Panthi and Samuel O. Odoh*

Department of Chemistry, University of Nevada Reno, 1664 N. Virginia Street, Reno, NV 89557-0216

Email Addresses:

curtisk@nevada.unr.edu

dpanthi@unr.edu

sodoh@unr.edu

Abstract: Copper-exchanged zeolites are useful materials for step-wise methane-to-methanol conversion (MMC). However, methanol yields on copper-exchanged zeolites are often modest, spurring interest in the development of active-site species that are activated at moderate temperatures, afford greater yields, and provide excellent methanol selectivities. Ultraviolet-visible, (UV-Vis) spectroscopy is a major tool for characterizing the active-sites and their evolution during the step-wise MMC process. However, computation of the UV-Vis spectra of the copper-oxo active sites using Tamm-Dancoff time-dependent density functional theory (TDA-DFT) can be quite problematic. This has led to utilization of expensive methods based on multi-reference approaches, Green functions and the Bethe-Salpeter equation. In this work, we examined the optical spectra of $[CuO]^+$, $[Cu_2O]^{2+}$, $[Cu_2O_2]^{2+}$ and $[Cu_3O_3]^{2+}$ species implicated in MMC in zeolites. For the larger species, we examined how agreement with experimental data is improved with increasingly larger cluster models. For $[CuO]^+$, we compared TDA-DFT against restricted active space 2nd-order perturbation theory, RASPT2. We found that signature peaks for $[CuO]^+$ have multi-reference behavior. The excited states have many configuration state functions with double excitation character. These effects are likely responsible for the poor utility of conventional TDA-DFT methods. Indeed, we obtain good agreement with experimental data and RASPT2 after accounting for 2h/2p excitations within TDA-DFT with a previously described configuration interaction singles and doubles, CIS(D)-style scheme. This was the case for $[CuO]^+$, $[Cu_2O]^{2+}$ as well as a $[Cu_2O_2]^{2+}$ species. Using a long-range corrected double-hybrid, ωB2PLYP, we provide for the first time, computational evidence for the experimental UV-Vis spectrum of the $[Cu_3O_3]^{2+}$ active site motif.

Keywords: Copper-exchanged zeolites, TD-DFT, methane, C-H bond activation, methanol, TD-DFT, long-range corrected double hybrids, double excitations

INTRODUCTION

Around the world, there are abundant deposits of natural gas. It is used in power generation as well as in the manufacture of intermediate chemicals. Due to difficulties associated with storage and transport, utilization of natural gas is sometimes limited to the area it is extracted. It is thus of economic and environmental interest to convert methane to liquid derivatives, such as methanol. Over the years, copper-exchanged zeolites have emerged as one of the most interesting species for converting methane to methanol.[1-7] They can be used at moderate temperatures (200 °C) where they generate up to 98% selectivities for methanol. Methane activation in these zeolites occurs on a set of copper-oxo active sites. As such, experimental characterization of these active-sites have helped to provide insights into the development of species that could provide improved yields and selectivities. Some experimental methods of characterization include X-ray diffraction, NMR, EPR, IR as well as resonant Raman spectroscopy. Additionally, it is quite common to compliment these empirical methods with computational chemistry approaches.[4,5,8]

For UV-Vis spectra, quantum-mechanical analyses are useful for interpreting experimental observations. Specifically, electronic structure calculations are useful for explaining the origins of peaks within empirical spectra. Electronic structure calculations of optical spectra can be performed with highly sophisticated approaches such as CASSCF[9] and coupled cluster methods[10]. However, as the systems of interest increase in size, it becomes more costly to run the highest quality calculations. As such, time-dependent density functional theory (TD-DFT[11]) has become a widely popular tool for predicting and analyzing absorption spectra and emission properties. This is largely due to the favorable accuracy-to-cost ratio of TD-DFT calculations.[12-14] However, TD-DFT calculations for metal-containing active sites often provide significant errors.[15-17] In many cases, these errors are due to intrinsic issues within TD-DFT with approximate density functionals. Some examples of these errors include ghost excitations, inaccurate treatment of charge-transfer excitations, problematic description of high-lying excited states as well as incorrect treatment of double excitations of electrons.[12,18-20] Another important consideration is the difficulty associated with open-shell systems with broken-symmetry electron configurations, necessitating the use of rigorously spin-adapted TD-DFT.[21-24]

Over the years, approaches to resolve some of the issues affecting TD-DFT have been developed. Nowadays, long-range corrected density functionals can provide excellent treatment of the charge-transfer excitations.[13,25,26] Approaches for treating double electron excitations within

the framework of TD-DFT have also been developed.[27-30] Some of these methods use approaches reminiscent of the perturbative treatment of doubles, CIS(D) developed by Head-Gordon et al. for CIS.[31] There are two major advantages for using the CIS(D) scheme. Firstly, CIS(D) energies are size-consistent. The CIS(D) method is also fairly affordable with an $O(N)^5$ scaling. Interestingly, the CIS(D) scheme was adapted for double-hybrid exchange-correlation functionals by Neese and Grimme.[27] In the original CIS(D) formulation, the excitation energies with perturbative doubles corrections are written as:

$$\omega^{CIS(D)} = E^{CIS(D)} - E^{MP2} = \frac{-1}{4}\sum_{ijab}\frac{\left(\bar{u}_{ij}^{ab}\right)^2}{\Delta_{ij}^{ab} - \omega} + \sum_{ia} b_i^a v_i^a \qquad (\mathbf{1})$$

where $\omega^{CIS(D)}$ is the doubles correction, $E^{CIS(D)}$ is the CIS(D) energy, E^{MP2} is the MP2 energy, $\mu^{-}{}_{ij}{}^{ab}$ are arrays as defined by ground state correlation theories, $\Delta^{ab}{}_{ij}$ is the difference between orbital eigenvalues *a* and *i* and *b* and *j* respectively, ω is the single excitation contribution, and $\sum_{ia} b_i^a v_i^a$ is the summation of the product of excited state amplitudes and their arrays. Grimme and Neese modified this for the B2PLYP double-hybrid functional[32] thus:

$$\omega_{TD(A)-B2PLYP} = \omega + a_c\Delta_{(D)} \qquad (\mathbf{2})$$

where ω is the single excitation contribution, and $a_c\Delta_{(D)}$ is the $\omega^{CIS(D)}$ correction. a_c is the coefficient of the electron correlation from second-order perturbation theory, MP2, in the original double hybrid functional.[27] Essentially, the CIS(D) correction to the excitation energies is scaled with the same coefficient for the MP2 correlation in the parent double hybrid functional, see **3**.

$$E_{xc} = (1 - a_X)E_X{}^{DFT} + a_X E_X{}^{HF} + (1 - a_C)E_C{}^{DFT} + a_C E_C{}^{MP2} \qquad (\mathbf{3})$$

Casanova-Paez et al. have extended this approach to long-range corrected double hybrid density functionals. ωB2PLYP and ωB2GP-PLYP are two examples.[33] Interestingly, ωB2PLYP performs well for the excited state properties of titanium dioxide clusters. It is therefore interesting to determine whether it is useful for predicting the optical spectra of copper-oxo species.

Despite the above-mentioned advances, TD-DFT has not found widespread usage for interpreting the UV-Vis spectra of copper-exchanged zeolites implicated in step-wise methane-to-methanol conversion, MMC. Woertink et al. computed the UV-Vis spectrum of the Cu_2O^{2+} species in ZSM-5.[34] They predicted a peak at 23400 cm^{-1}, in good agreement with the band observed at 22700 cm^{-1}. More recently, Göltl et al. computed the absorption and photoluminescence spectra of Cu(I) sites in the SSZ-13 zeolite while using a time-dependent hybrid Hartree-Fock-like linear response scheme. The amount of Hartree-Fock exchange was parameterized by comparing a specific

transition to experimental measurements.[1] Thereafter Göltl et al. obtained excellent agreement for other transitions. Interestingly, Ipek et al. computed the optical spectra of copper-oxo active sites with Green functions-based methods as well as the Bethe-Salpeter equation.[35] Given, the expensive nature of these methods, we here consider the performance of TD-DFT for predicting the spectra of copper-oxo active site motifs implicated in MMC.

In this work, we have carried out a systematic examination of TD-DFT using various classes of density functionals for understanding the UV-Vis spectrum of the $[CuO]^+$, $[Cu_2O]^{2+}$, $[Cu_2O_2]^{2+}$ and $[Cu_3O_3]^{2+}$ species. For these systems, we used small cluster models possessing aquo ligands around the copper-oxo sites. In the cases of the $[Cu_2O]^{2+}$ and $[Cu_2O_2]^{2+}$, we gradually expanded the cluster models by including nearby aluminate tetrahedra that anchor the active sites within zeolites. This allowed us to determine the extent to which TD-DFT spectra of the copper-oxo sites depend on the size of the cluster models. Specifically, we first compare TD-DFT to restricted active space second-order perturbation theory, RASPT2, for the mono-copper system: CuO^+. We used one of the best performing functionals for CuO^+ to study the other active site motifs.

2 METHODOLOGY

2.1. Geometry Optimizations: The aquo complexes of $[Cu_2O]^{2+}$ and $[Cu_2O_2]^{2+}$ are shown in Figure 1. With these aquo complexes, we can more easily identify electronic excitations due to the copper-oxo active sites. All these and CuO^+ were optimized with the B3LYP functional while accounting for dispersion effects with the D3 scheme[36,37] and Becke-Johnson damping method.[38] We used def2-TZVPP basis sets for all geometry optimizations. For the mono-(μ-oxo) dicopper $[Cu_2O](H_2O)_2^{2+}$ complex, we fixed the Cu-O-Cu bond angle at 140°. This is the experimental value for this structural parameter in zeolite ZSM-5.[8,34] Overall, the ground states for our $[Cu_2O]^{2+}$ and $[Cu_2O_2]^{2+}$ cluster models are open-shell singlet states while for our $[Cu_3O_3]^{2+}$ model, the ground state is a doublet, see Supporting Information, SI.

2.2. TD-DFT Calculations: All TD-DFT calculations were performed with the Tamm-Dancoff approximation[39] (TDA-DFT) while using the ORCA v4.2.1 software code.[40,41] For CuO^+ and the $[Cu_2O_2]^{2+}$species of interest, we used 21 DFT functionals for the TDA-DFT calculations. These include GGAs and meta-GGAs (BLYP[42,43], PBE[44], PW91[45], mPWLYP, M06L[46] and TPSS[47]), hybrids and meta-hybrids (B3LYP[48-50], M06, M062X[51], O3LYP[52,53], PBE0[44,54], TPSS0[47] and TPSSh[47]) and long-range corrected functionals (CAM-B3LYP[55], LC-BLYP[56] and ωB97X[57]).

In addition, we carried out TDA-DFT calculations with double-hybrid functionals which used the CIS(D)-style approach of Grimme and Neese[27]. These are referred to as B2PLYP[32], B2GP-PLYP[58], mPW2PLYP[59], ωB2PLYP[33] and ωB2GP-PLYP[33], respectively. Several workers have reported extensive benchmarks of TDA-DFT with double-hybrid density functionals.[27,60] The truncated hybrid-GGA solutions used in these double-hybrid functionals are referred to as B2LYP, B2GP-LYP, mPW2LYP, ωB2LYP and ωB2GP-LYP, respectively.[61-63]

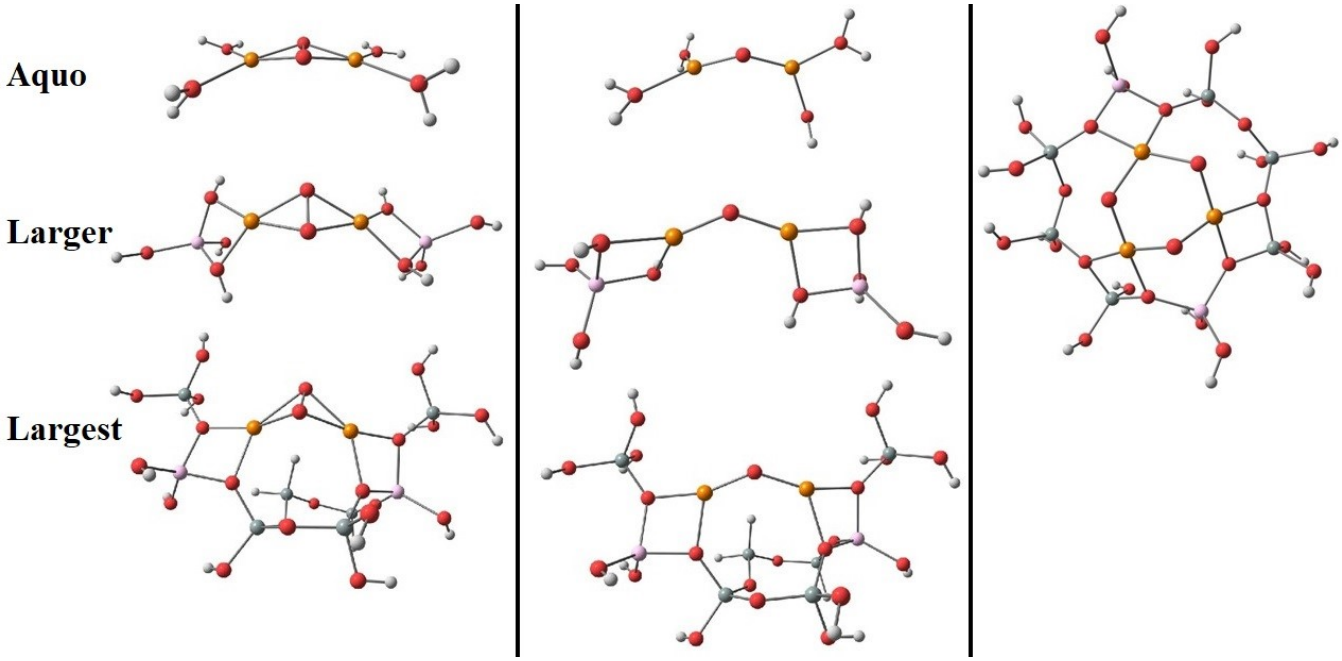

Figure 1: Cluster models of the **(Left)** μ-(η^2:η^2) bent-peroxo dicopper $[Cu_2O_2]^{2+}$ **(middle)** mono-(μ-oxo) dicopper $[Cu_2O]^{2+}$ and **(right)** tris-(μ-oxo) tricopper $[Cu_3O_3]^{2+}$ active site motifs. For the dicopper species, the aquo, larger and largest cluster models are shown from top to bottom.

The resolution of identity and chain-of-spheres approximation, RIJCOSX, was employed for all TDA-DFT calculations.[64,65] These were generally performed with aug-cc-pVTZ basis sets[66] while using def2-TZVP/C resolution of identity (RI) auxiliary correlation basis sets for the RI-MP2 portions of the double hybrids and long-range corrected double hybrids.[67] We checked the sensitivity of our conclusions to basis set choices and sizes, see SI. TDA-DFT calculations on the largest cluster models were performed with cc-pVDZ basis sets. For TDA-DFT, we performed all calculations requesting 60- 200 states. Unrestricted determinants were used throughout. Except when noted otherwise, all spectra were fitted with a Lorentzian function with a 1200 cm^{-1} width.

2.3. Multi-Reference Treatment of CuO^+: State-average restricted active space self-consistent field, SA-RASSCF, and multi-state RASPT2[27-30], MS-RASPT2, calculations on CuO^+ were performed with the OpenMolcas code.[68,69] CuO^+ is used as a model system, as its size allows

for a quite good treatment with multi-reference methods. Interestingly, Kulkarni et al. recently proposed CuO^+ as a possible monocopper active site motif for MMC in copper-exchanged zeolites.[70] For RASSCF and RASPT2, we used the ANO-RCC-VTZP[71,72] basis sets in addition to a second-order Douglas-Kroll-Hess treatment of scalar-relativistic effects.[73] For RASSCF, we used an active space (RAS2) consisting of 14 electrons in 9 orbitals while using an outer active space (RAS3) containing 8 empty orbitals. A maximum of two electrons were allowed in RAS3 while all possible excitations were considered for RAS2. The RAS2 orbitals are the 3d orbitals of Cu, the 2p orbitals of O and the 4s orbital from Cu. For RAS3, we used the double-shell orbitals, specifically the 4d orbitals of Cu and the 3p orbitals of O. This partitioning of the active space is shown in Figure 2. All our calculations and analysis were performed with the C2v symmetry point group on the triplet state of CuO^+. We considered 12 electronic states, the ground state and 11 excited states.

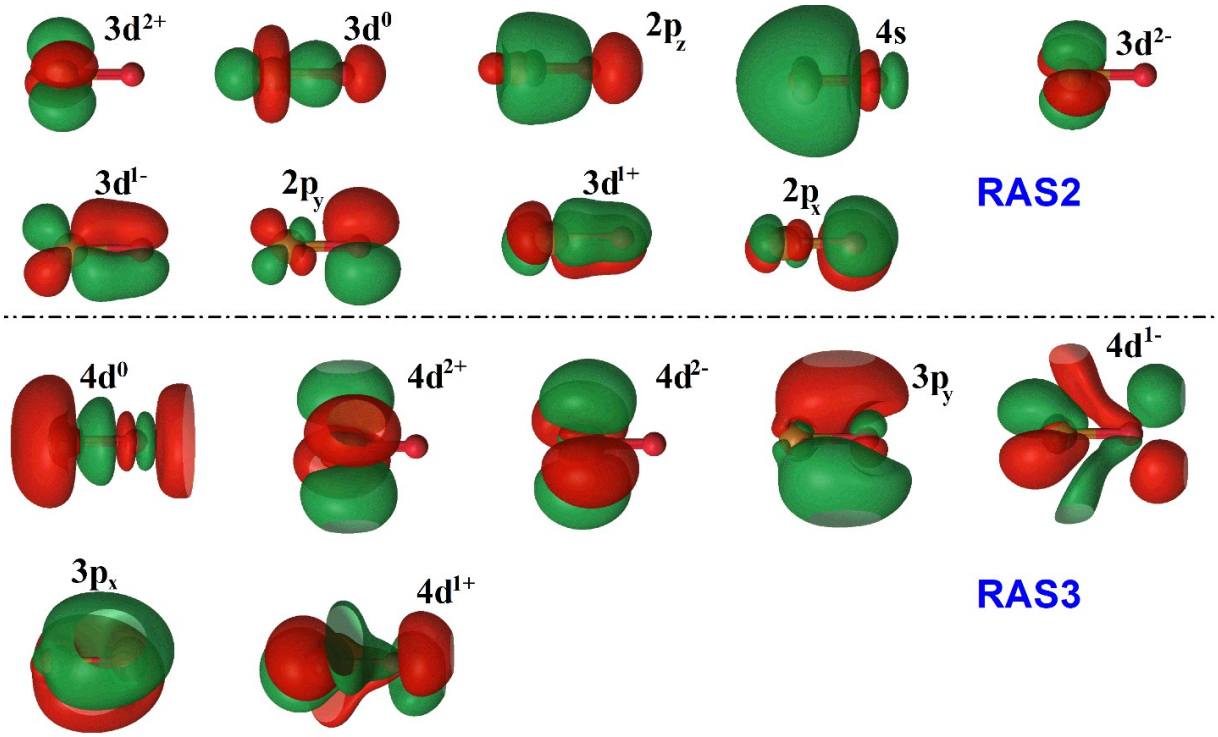

Figure 2: Active space orbitals for CuO^+. RAS2 space is on the top while the RAS3 space is on the bottom. The dominant atomic contributions to the molecular orbitals are given.

For MS-RASPT2, we did not use the IPEA shift (0.0 eV)[74] but we used an imaginary shift of 0.2 a.u. (5.44 eV) to account for intruder states.[75] The intensities of the calculated electronic excitations were obtained with the restricted active space state interaction, RASSI, module of OpenMolcas while using the spin-free effective Hamiltonian, adding in dynamic correlation from RASPT2.[68,69]

3 RESULTS AND DISCUSSIONS

3.1. Multi-Reference and TDA-DFT Results for CuO^+: The computed UV-Vis spectra of CuO^+ from with SA-RASSCF and MS-RASPT2 are shown in Figure 3. SA-RASSCF predicts two peaks

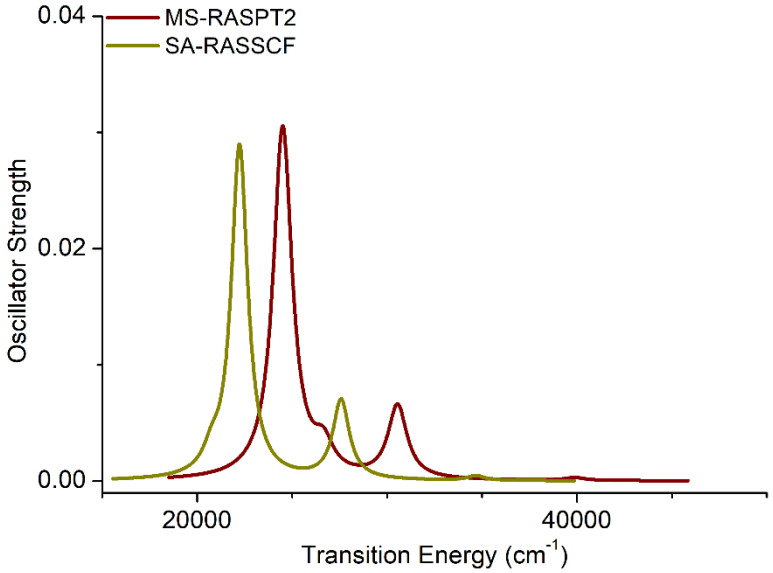

Figure 3: Region around 20000 and 40000 cm^{-1} in the UV-Vis spectra of CuO^+ system obtained with SA-RASSCF and MS-RASPT2.

at 22232 and 27582 cm^{-1}. These are shifted to 24505 and 30547 cm^{-1} after inclusion of dynamic correlation effects with MS-RASPT2. Analysis of the SA-RASSCF wavefunction reveals that the two dominant peaks correspond largely to excitations from doubly-occupied 3d-dominated molecular orbitals to singly-occupied orbitals dominated by the 2p atomic orbitals of the O atom. However, the dominant configuration in the ground state wavefunction has a weight of 68.3%, with 17.8% also coming from configuration state functions (CSF) corresponding to excitations from $3d^{1+}$ or $3d^{1-}$-dominated orbitals to singly-occupied $2p_y$ or $2p_x$ orbitals on O. This indicates that the ground state is significantly multi-reference. Our analysis agrees well with that of Srnec et al.[76] The excited state wavefunctions for these peaks also have significant multi-reference characters. Their dominant CSFs have weights of 19.6 and 48.5%. These CSFs are formed from $3d^{1+} \rightarrow 2p_y$ excitations from the dominant CSF of the ground state. The excited states also have appreciable contributions (18.7% and 23.3%) from CSFs corresponding to 3d → 4s excitations. Relative to the dominant ground state CSF, these correspond to double excitations. Thus, good treatment of static and dynamical correlation is crucial for accurate prediction of the UV-Vis spectrum of CuO^+. Also, double excitations will play a major role in the characters of the excited

states.

The TDA-DFT spectra of CuO^+ obtained with BLYP, B3LYP, CAM-B3LYP and B2PLYP while using aug-cc-pVTZ basis sets are compared to MS-RASPT2 in Figure 4. The most intense 3d → 2p and 3d → 3d excitations in the TDA-DFT spectra are found around 40000 cm^{-1}. These greatly overestimate the excitation energies obtained with the multi-reference methods. The spectral shape as well as intensities of the peaks around 40000 cm^{-1} are also quite different from that of SA-RASSCF and MS-RASPT2. Specifically, the intensities of the dominant bands from TDA-DFT are sometimes nearly twice that from the multi-reference methods. Thus, TDA-DFT not only predicts the wrong excitation energies, it also significantly overestimates the band intensities. The poor performance of these functionals is certainly not due to the basis set sizes. The B3LYP spectra remains unchanged when we used def2-SVP, cc-pVDZ, def2-TZVP, ma-def2-TZVPP, cc-pVTZ, aug-cc-pVDZ and aug-cc-pVQZ basis set, see SI. Additionally, this poor performance extends to all the DFT functionals that we tested. We therefore conclude that the poor performance of TDA-DFT relative to MS-RASPT2 is not a result of basis set limitations or an inaccurate treatment of charge transfer excitations or Rydberg excitations.

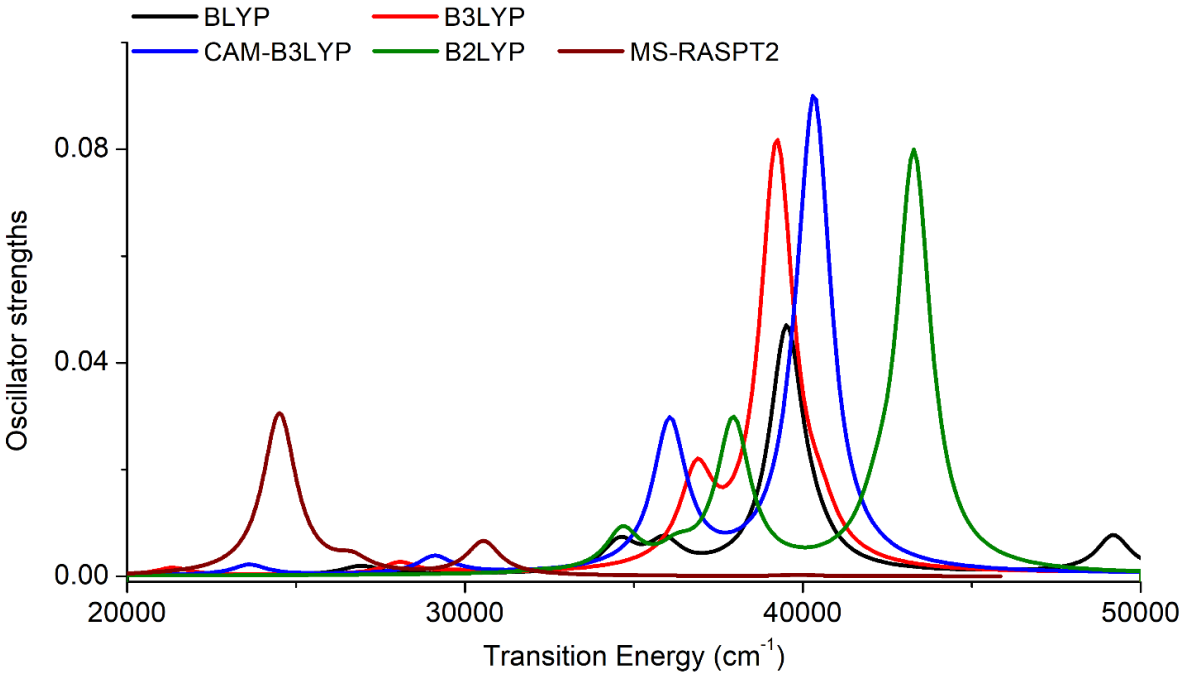

Figure 4: Region around 20000-50000 cm^{-1} in the UV-Vis spectra of CuO^+ system obtained with TDA-DFT and MS-RASPT2.

Interestingly, we found that the double-hybrid density functionals are quite close to MS-RASPT2 and SA-RASSCF, Figure 5. Specifically, the peaks at 35000-50000 cm^{-1} for hybrid functionals

now appear at 15000-30000 cm^{-1} for the double hybrid functionals. As an example, excitations at 37940 and 43288 cm^{-1} with B2LYP are shifted to 22107 and 20014 cm^{-1} with B2PLYP. Also, for B2PLYP the spectral shapes and intensities of the peaks around 20000 cm^{-1} match well with results from multi-reference calculations. The observed red-shift due to the CIS(D) correction in the double hybrid density functionals have been previously described.[27,61-63]

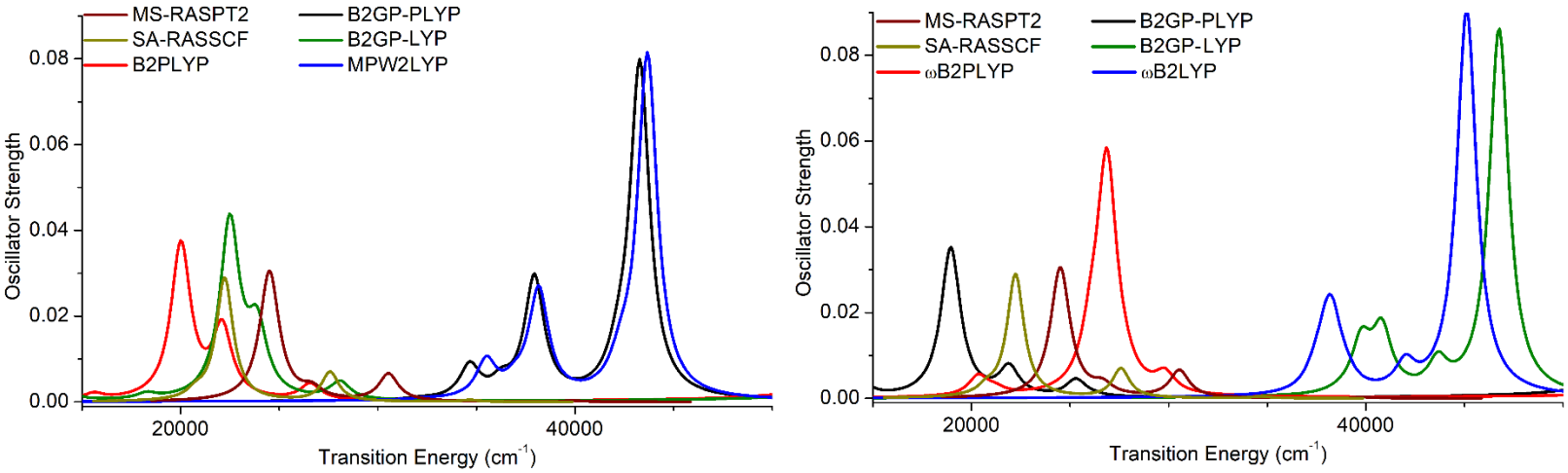

Figure 5: Region around 20000-50000 cm^{-1} in the UV-Vis spectra of CuO^+ obtained with double excitations-corrected TDA-DFT and MS-RASPT2.

By comparing the peak positions of the major TDA-DFT excitations in the 15000-50000 cm^{-1} region to MS-RASPT2, we can evaluate the performance of DFT functionals. The results of these analyses are presented in Table 1. Overall, the GGAs, meta-GGAs, hybrids, meta-hybrids and

Table 1: Mean absolute deviations (MAD) and mean signed deviations (MSD), in eV, of the dominant and smaller peaks in the TDA-DFT spectra from MS-RASPT2.

	PBE	B3LYP	M06L	M06	mPW2LYP	mPW2PLYP	B2LYP	B2PLYP
MSD	1.59	1.63	1.94	1.73	1.48	-0.21	1.41	-0.48
MAD	1.59	1.63	1.94	1.73	1.48	0.25	1.41	0.48

range-separated hybrids perform very poorly. They deviate from MS-RASPT2 by up to 2.0 eV. The truncated hybrid GGAs, B2LYP, B2GP-LYP, mPW2LYP, ωB2LYP and ωB2GP-LYP, also perform poorly. Good agreement with MS-RASPT2 is only achieved after inclusion of corrections for double excitations in the double hybrid functionals. B2PLYP and mPW2PLYP have mean absolute deviations, MADs, of 0.48 and 0.25 eV, respectively. B2GP-PLYP, ωB2GP-PLYP and ωB2PLYP also do fairly well with MADs of 0.56, 0.57 and 0.38 eV, respectively. As such, we

have evaluated the performance of ωB2PLYP for several copper-oxo active-site motifs implicated in MMC.

3.2. UV-Vis Spectrum of μ-(η^2:η^2) bent-peroxo Dicopper $[Cu_2O_2]^{2+}$: Ipek et al. reported that the bent μ-(η^2:η^2) peroxo dicopper motif has a broad band at 27800 cm^{-1} in the SSZ zeolite.[35] This was considered to be due to peroxo to Cu(II) charge transfer excitations. They also assigned features at 20400-23800 cm^{-1} as well as a very weak feature at 18200 cm^{-1} to this active site.[35]

3.2.1. ***Aquo complex:*** Given the previous description of the band at 27800 cm^{-1} as a charge transfer band, we first considered the performance of CAM-B3LYP and LC-BLYP for the tetra-aquo complex, μ-(η^2:η^2) bent-peroxo dicopper $[Cu_2O_2](H_2O)_4^{2+}$, Figure 1. These functionals predict the broken-symmetry open-shell singlet state to be more stable than the triplet state by 2.4 and 2.1 kcal/mol respectively. We however realize that it is possible that the zeolite framework could reduce the energy gap between these two states. Thus, the TDA-DFT spectra of both states were considered, Figure 6. The CAM- B3LYP and LC-BLYP spectra of the singlet state have only one intense feature in the region between 10000 and 50000 cm^{-1}. With CAM-B3LYP, this peak is at

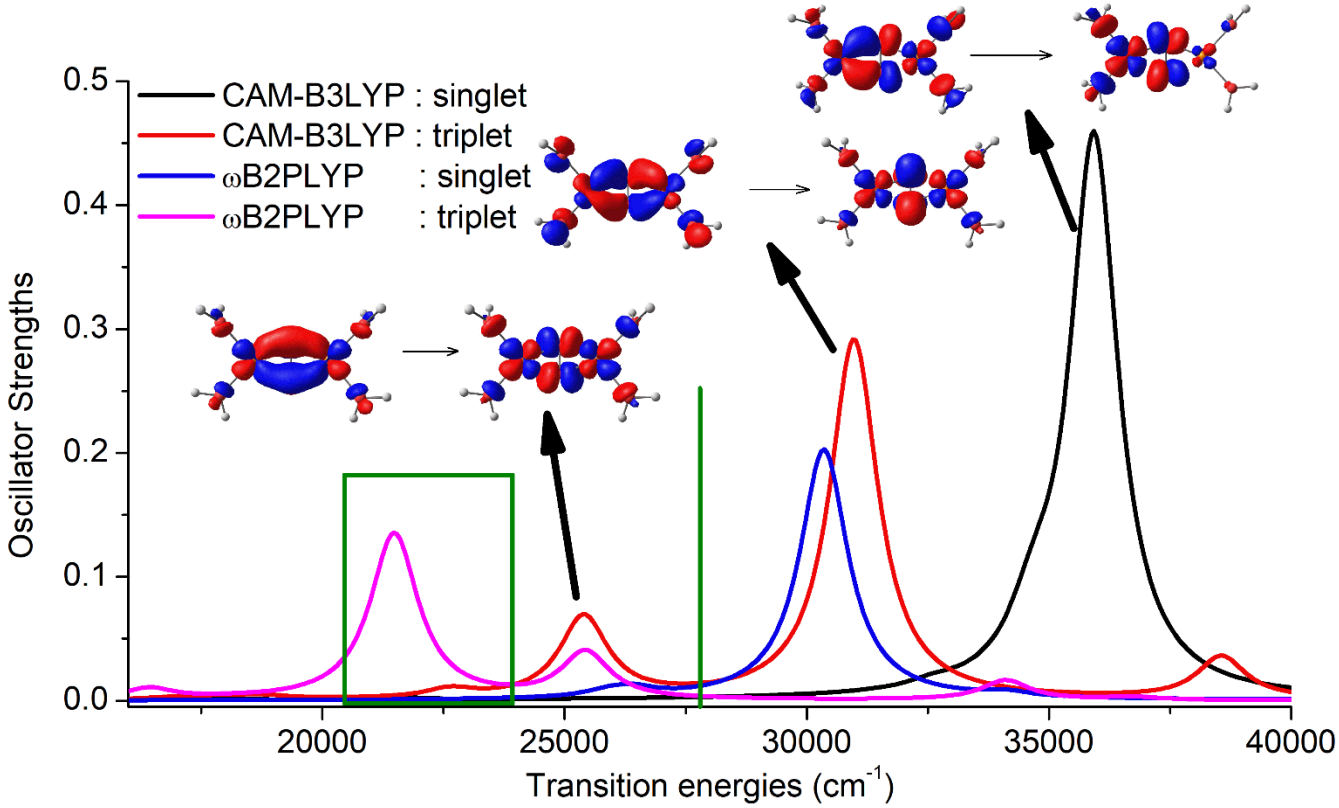

Figure 6: Calculated TDA-DFT spectra of the μ-(η^2:η^2) bent-peroxo dicopper $[Cu_2O_2](H_2O)_4^{2+}$ aquo complex. Experimental estimates for this motif in zeolites are shown in green lines or boxes.

35925 cm^{-1}, while with LC-BLYP, it is at 37212 cm^{-1}. These peaks are due to molecular orbitals involving 3d orbitals of the metal centers and 2p orbitals of the peroxo oxygen atoms, Figure 6. They also have significant contributions from the 2p orbitals of the aquo ligands.

Turning to the triplet state, we see moderately intense peaks at 25396, 30972 and 38556 cm^{-1} in the CAM-B3LYP spectra, Figure 6. These peaks all have significant Cu-O_2-Cu $\pi \rightarrow \pi^*$ characters. Also, they are fairly close to the experimental peaks at 27800 and 20400-23800 cm^{-1}.

With ωB2PLYP, we find that the more stable singlet state has a single dominant peak at 30350 cm^{-1}, about 2550 cm^{-1} (0.28 eV) from the experimentally observed broad band at 27800 cm^{-1}. The triplet state has significant Cu-O_2-Cu $\pi \rightarrow \pi^*$ transitions at 21484 and 25432 cm^{-1}. These are close to the experimental assignments at 20400-23800 cm^{-1}. However, taking together the singlet- and triplet-state results, we conclude that the aquo complex is not a suitable model for the μ-(η^2:η^2) bent-peroxo dicopper active site motif. The intense transitions in the singlet state spectra are particularly problematic.

3.2.2. ***Larger model:*** With a charge-neutral and larger cluster model, Figure 1, the triplet state of the bent-peroxo $[Cu_2O_2]^{2+}$ active site motif is about 1.9 kcal/mol above the singlet state at the B3LYP-D3BJ/def2-TZVPP level. Interestingly, the singlet state active site is more stable than the triplet state by only 1.0 kcal/mol in the 8MR of zeolite MOR. This was obtained from periodic DFT calculations while using the PBE-D3 density functional.[36,44] Details of the periodic DFT calculations are given in the SI.

With the larger cluster model, B3LYP, CAM-B3LYP and LC-BLYP still do not yield spectra in good agreement with experiments. This is because they still predict an intense feature around 30000-32000 cm^{-1} for the singlet state. The experimental assignments are only for features below 27800 cm^{-1}, Figure 7. By contrast, with ωB2PLYP, there is a strong feature at 27884 cm^{-1} in the TDA-DFT spectrum of the singlet state, matching quite well with the experimental feature at 27800 cm^{-1}. In the triplet state, the dominant feature is at 20652 cm^{-1}, again matching the experimental assignment at 20400-23800 cm^{-1}, Figure 7. However, these do not provide any peaks around 18200 cm^{-1}, as assigned by Ipek et al.

3.2.3. ***Largest model:*** For the largest cluster model incorporating the full first-coordination sphere around the bent-peroxo $[Cu_2O_2]^{2+}$ active site motif, the singlet state has an intense peak at 26621, 27137 cm^{-1}, respectively, in the spectra obtained with B3LYP and CAM-B3LYP. These agree

excellently with Ipek et al.'s assignment of the feature at 27800 cm^{-1} to this moiety. For the triplet state, similar intense peaks are seen at 26796 and 27009 cm^{-1} for these functionals respectively,

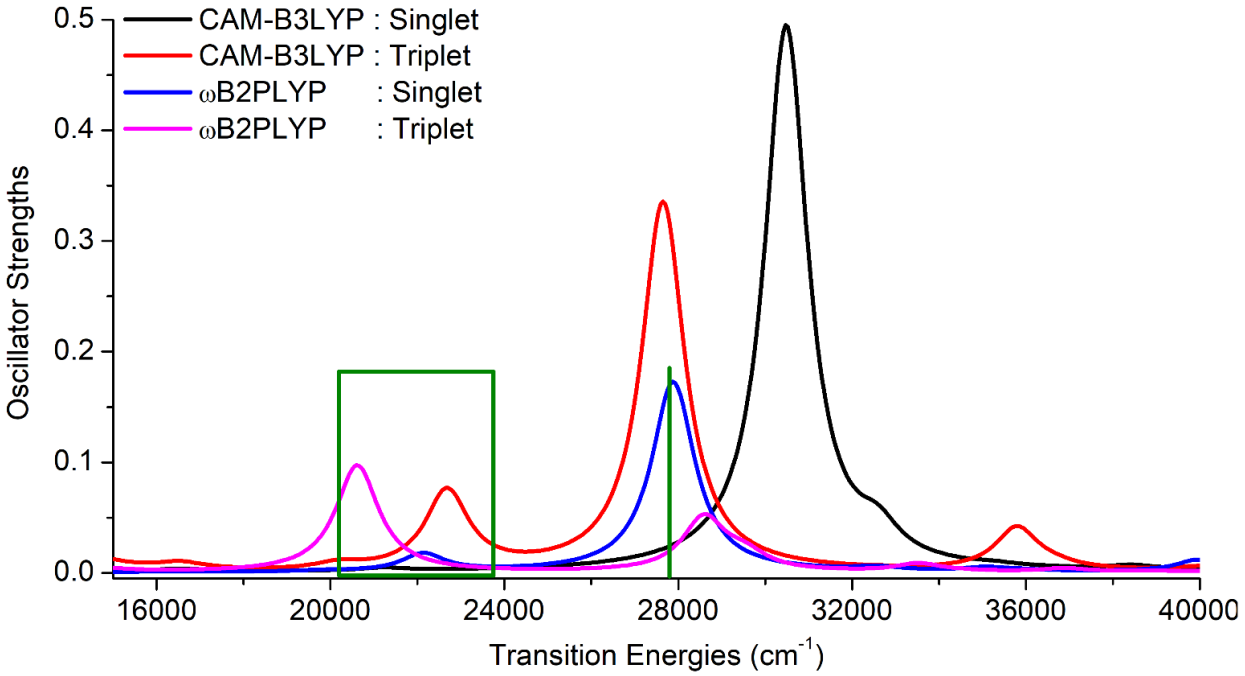

Figure 7: Region around 16000-40000 cm^{-1} in the UV-Vis spectra of the larger cluster model of the μ-(η^2:η^2) bent-peroxo dicopper $[Cu_2O_2]^{2+}$ active site. The experimental estimates for this motif in zeolites are shown with green lines or boxes.

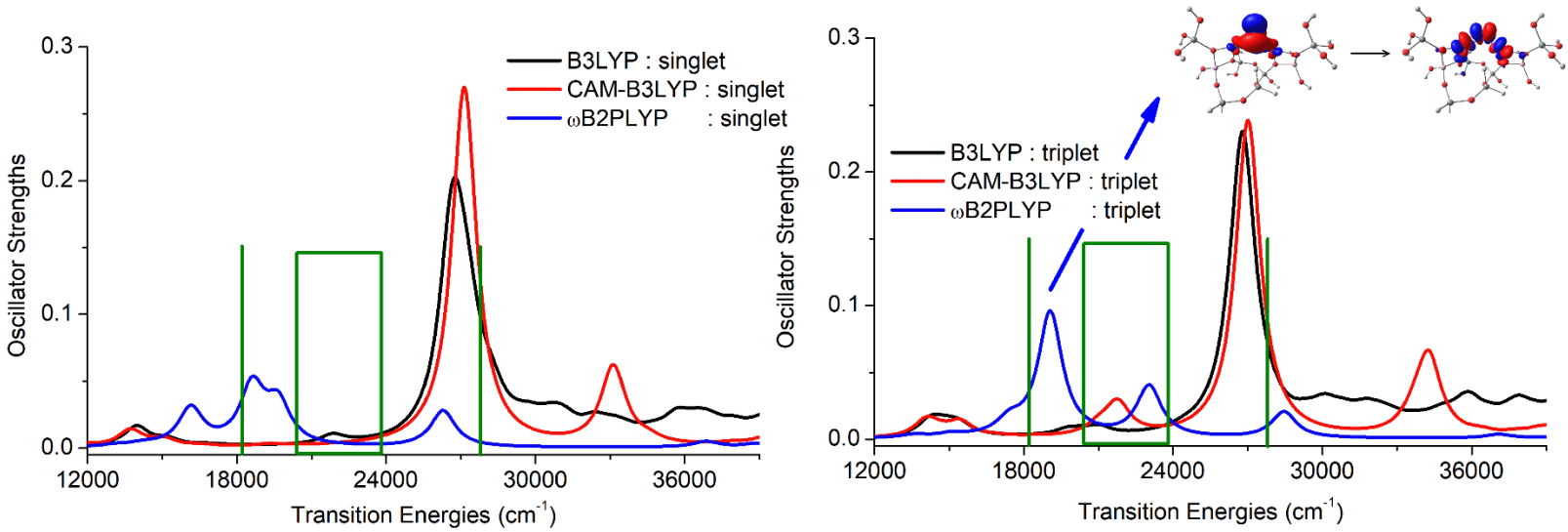

Figure 8: Region around 16000-40000 cm^{-1} in the UV-Vis spectra of the largest cluster model of the μ-(η^2:η^2) bent-peroxo dicopper $[Cu_2O_2]^{2+}$ active site. The experimental estimates for this motif in zeolites are shown with green lines or boxes.

Figure 8. Thus, using this 48-atom cluster model removes the problematic nature of peaks around 30000 cm^{-1} in the smaller cluster model calculations with B3LYP and CAM-B3LYP, Figure 7. However, these functionals provide no opportunity for agreement with Ipek et al.'s assignment of features at 18200 and 20400-23800 cm^{-1} to this active site motif, Figure 8. For this reason, we shall turn to ωB2PLYP. In the singlet state, this method provides peaks at 26297, 19602, 18661 and 16227 cm^{-1}. For the triplet state, this approach yields peaks at 19062, 23031 and 28450 cm^{-1}. The predicted peaks for both states are within 2000 cm^{-1} (0.25 eV) of Ipek et al.'s assignment at 27800, 20400-23800 and 18200 cm^{-1} to this motif, Figure 8.

3.3. UV-Vis Spectrum of Mono-(μ-oxo) Dicopper $[Cu_2O]^{2+}$: The broad feature at 22700 cm^{-1} in the absorption spectrum of activated Cu-ZSM-5 has been used to monitor the kinetics of methane hydroxylation.[34] Additionally, this signature of the $[Cu_2O]^{2+}$ active site has been observed at 21900 and 23100 cm^{-1} in the MOR zeolite.[77] Through a combination of UV-Vis and resonance Raman spectroscopy, these features can be definitively assigned to the mono-(μ-oxo) dicopper, Cu_2O^{2+} active site motif.[8]

3.3.1. ***Aquo complex:*** The Cu-O-Cu bond angle of the Cu_2O^{2+} active site motif was found to be 140° in the 10MR of zeolite ZSM-5. As such, we optimized the structures of $[Cu_2O](H_2O)_4^{2+}$ in the singlet and triplet states while constraining the Cu-O-Cu angle to 140°. Our ground state calculations indicate that the singlet and triplet states are rather close in energy, 2.7 kcal/mol at the B3LYP-D3BJ/def2-TZVPP level in favor of the triplet state.

With B3LYP, there are two intense features centered on 28000 and 36000 cm^{-1} in the TDA-DFT spectrum of the triplet state. These features have rather complicated origins due to the heavily mixed natures of the orbitals involved. However, they both possess substantial oxo 2p → 3d charge-transfer characters. Only one feature is seen in the TDA-DFT spectrum obtained with CAM-B3LYP, at 26830 cm^{-1}. Overall, the lower-energy peaks in the TDA-DFT spectra of the triplet state are somewhat near the experimental peak at 22700 cm^{-1}, see SI.

Turning to ωB2PLYP, the TDA-DFT spectra of the singlet and triplet states have only one major peak below 40000 cm^{-1}. These are at 20971 cm^{-1} for the singlet and 20809 cm^{-1} for the triplet, see SI. Overall, the peaks obtained for $[Cu_2O](H_2O)_4^{2+}$ with ωB2PLYP are reasonably close to the experimentally observed feature at 22700 cm^{-1} (within 1729 cm^{-1} or 0.21 eV). We now seek to determine whether the good performance of B3LYP and ωB2PLYP extend to larger cluster models of the Cu_2O^{2+} active site.

3.3.2. *Larger model:* With a larger cluster model, Figure 1, the triplet state of $[Cu_2O]^{2+}$ is just 0.7 kcal/mol more stable than the singlet state. This was obtained at the B3LYP-D3BJ/def2-TZVPP level. When we used periodic PBE-D3 DFT approach to optimize the structure of $[Cu_2O]^{2+}$ in the 8MR of MOR, the singlet state is more stable than the triplet by 0.6 kcal/mol. These results suggest that both states will contribute significantly to the UV-Vis spectrum of the $[Cu_2O]^{2+}$ active site. Using the larger model, the signature peak of the $[Cu_2O]^{2+}$ active site is predicted by B3LYP to be centered at 23654 cm^{-1} for the singlet state and 25081 cm^{-1} for the triplet state, Figure 9. These are however rather broad peaks, due to the presence of several intense transitions in the 22000-28000 cm^{-1} range. As such, we can say that B3LYP performs moderately well for this active site. This is in accordance to the report of Woertink et al.[34] It is interesting that ωB2PLYP yields a dominant feature at 26124 cm^{-1} in the singlet state and 25876 cm^{-1} for the triplet state, Figure 9.

3.3.3. *Largest model:* With the largest cluster model used for the $[Cu_2O]^{2+}$ active site, we see that all functionals now predict only one dominant peak in the 20000-40000 cm^{-1} region, Figure 10. This shows that the 47-atom cluster model encompassing the full first-coordination environment is necessary for accurate spectra. That said B3LYP still indicates a broad feature with modest intensity around 32000 cm^{-1} for the triplet state, Figure 10. This is absent from the CAM-B3LYP

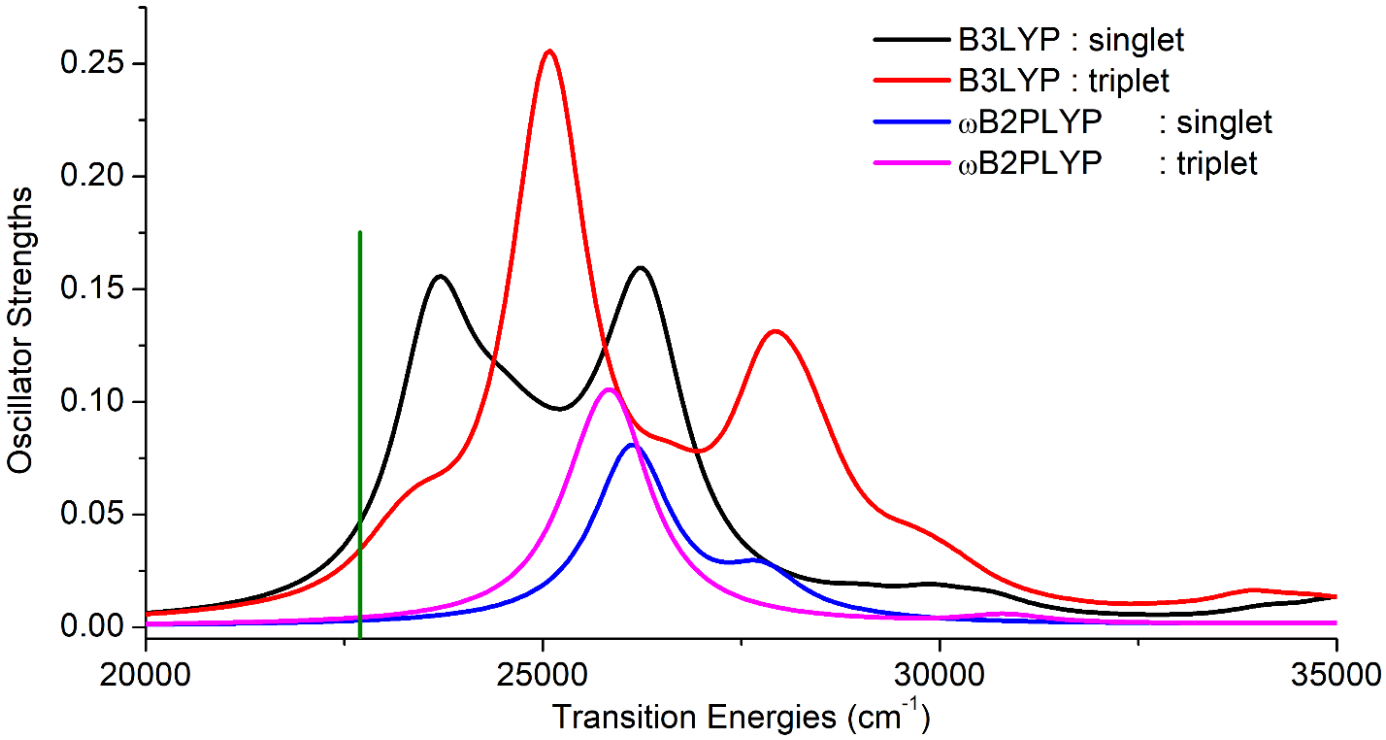

Figure 9: Regions around 20000-40000 cm^{-1} in the TDA-DFT spectra of the larger cluster model of mono-(μ-oxo) dicopper $[Cu_2O]^{2+}$. Experimental estimates are shown with a green line.

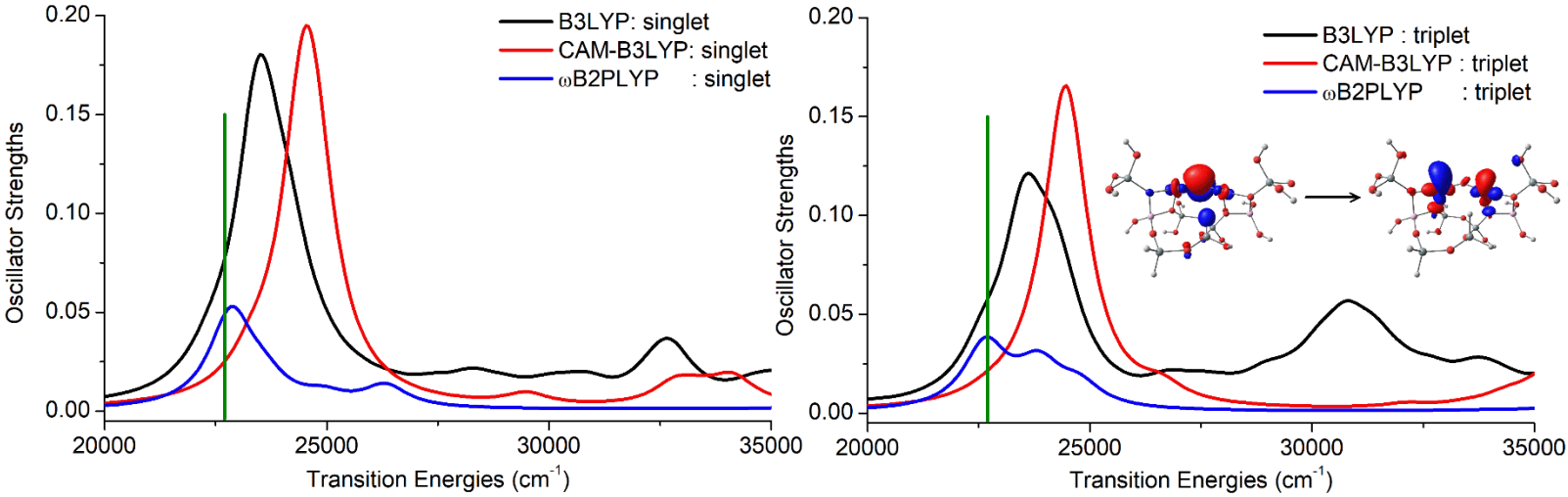

Figure 10: Regions around 20000-40000 cm^{-1} in TDA-DFT spectra of the largest cluster model of mono-(μ-oxo) dicopper $[Cu_2O]^{2+}$. The experimental assignment is shown with a green line.

and ωB2PLYP spectra. Focusing on the 22700 cm^{-1} signature peak in the experimental reports, ωB2PLYP is within 189 cm^{-1} for the singlet state and 44 cm^{-1} for the triplet state. Our calculations thus indicate that ωB2PLYP performs quite well for the $[Cu_2O]^{2+}$ active site, Figure 10. Analysis of the Kohn-Sham orbitals reveals that these excitations are of μ-oxo 2p → Cu (4s and 3d) charge transfer character, see inset of Figure 10.

3.4. UV-Vis Spectrum of Tris(μ-oxo) Tricopper $[Cu_3O_3]^{2+}$: Vogiatzis et al. and some of us have used DFT and wavefunction theory methods and various cluster models to compare the relative energies of the doublet and quartet states of the $[Cu_3O_3]^{2+}$ active site.[78-80] Overall, many of the wavefunction theory methods indicate that the doublet state is more stable than the quartet.

The experimental UV-Vis spectra of the $[Cu_3O_3]^{2+}$ active site in MOR shows several interesting features.[3,81] First, there is a peak centered at around 12000 cm^{-1}. There are no features around 20000-23000 cm^{-1}. There are also features at 32000, 34000 and 38500 cm^{-1}. These set of features make it challenging for excited-state computational chemistry methods. As such, there has been no computational evidence for the UV-Vis spectra of the $[Cu_3O_3]^{2+}$ motif. To illustrate, we present the calculated UV-Vis spectra of our cluster model[80] in Figure 11. We convoluted these spectra with Lorentzian functions with full width at half maximum of 3500 cm^{-1}.

According to B3LYP, the doublet state shows a weak feature at around 12200 cm^{-1} and other weak bands near 25000 cm^{-1}. Lastly, there is a large increase in intensity starting from around 30000 cm^{-1}. The feature at 12200 cm^{-1} is due to charge transfer from orbitals dominated by μ-oxo $2p_y$

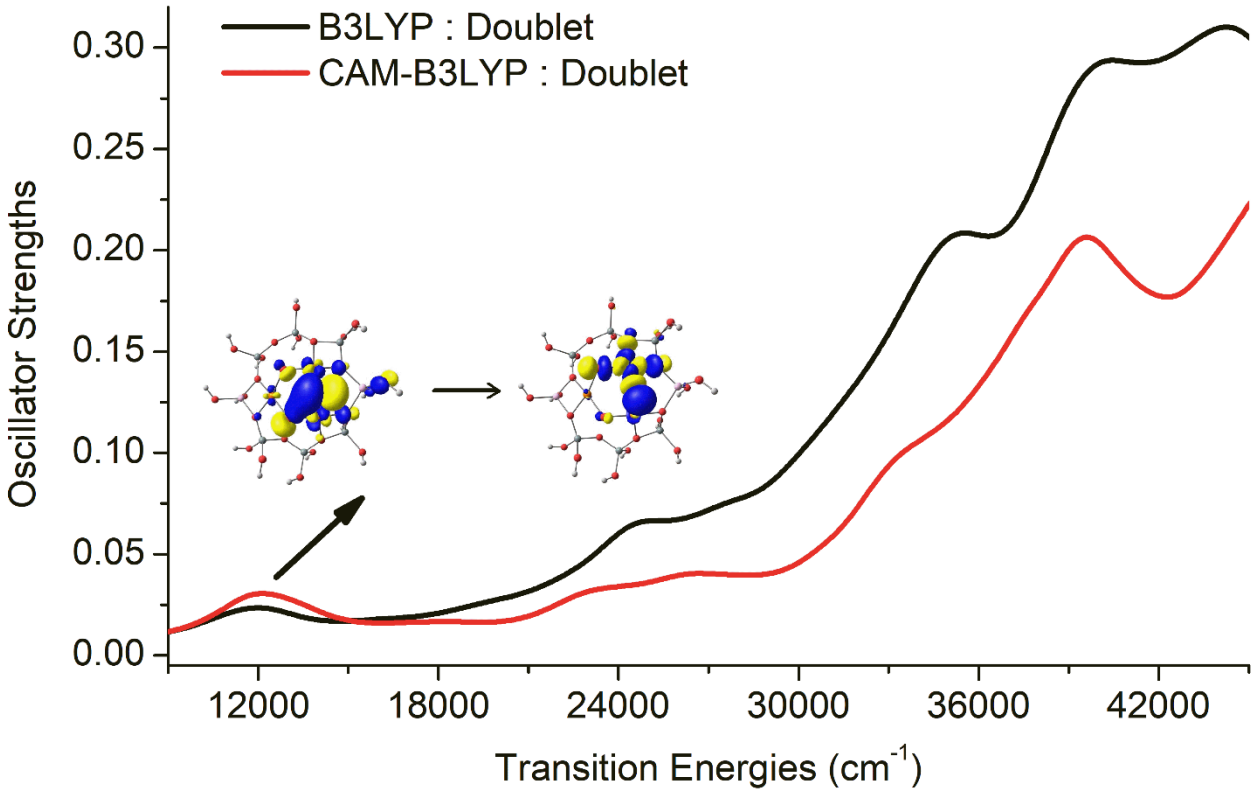

Figure 11: Region around 10000-40000 cm^{-1} in the TDA-DFT spectra of the $[Cu_3O_3]^{2+}$ cluster model obtained with the B3LYP and CAM-B3LYP density functionals for the doublet state.

atomic orbitals to those dominated by μ-oxo $2p_x$ and Cu 3d atomic orbitals, Figure 11. Thus, this transition is associated with charge transfer from one portion of the $[Cu_3O_3]^{2+}$ core to the other. There TDA-DFT spectrum from CAM-B3LYP is very similar to that from B3LYP, Figure 11. Again, there are only weak features near 12000 and 25000 cm^{-1}. Interestingly, with ωB2PLYP, we see a good agreement with the experimental results. Indeed the TDA-DFT spectrum for the low-spin state of our $[Cu_3O_3]^{2+}$ cluster model achieves all signature features of the experimental data, Figure 12. First, there is a peak at 14560 cm^{-1}. This is quite close to the peak near 12000 cm^{-1} in the experimental spectra. Second, there are no significant features near 20000-23000 cm^{-1}. This also concurs with the experimental data and precludes overlap with the signature feature of $[Cu_2O]^{2+}$ at 22700 cm^{-1}. Lastly, the calculated spectrum of the doublet state has features at 30110, 34408 and 36557 cm^{-1}, Figure 12. These match quite well to experimental features observed at 31000, 34000 and 38500 cm^{-1} by Kim et al.[3] and Grundner et al.[81] Interestingly, in our calculations, there is a peak at 25191 cm^{-1}. This agrees quite well with the report of Ikuno et al. who reported of a shoulder near 24000 cm^{-1}.[82]

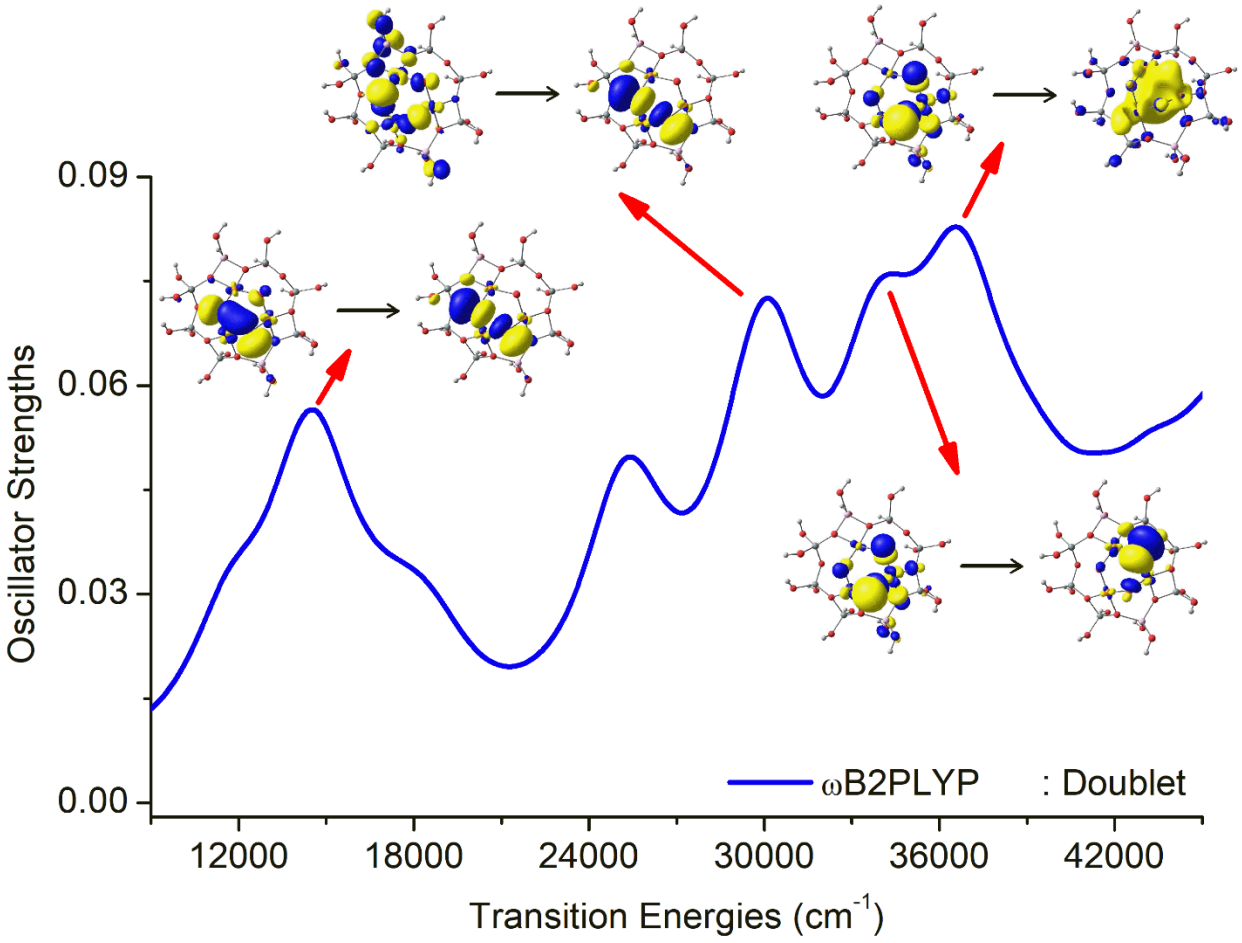

Figure 12: Region around 10000-40000 cm^{-1} in TDA-DFT spectra of $[Cu_3O_3](H_2O)_6^{2+}$ obtained at the ωB2PLYP/cc-pVDZ level.

The features in the spectrum have rather complicated origins, except for the dominant transition at 14560 cm^{-1}. This transition has the identical character to the peaks near 12200 cm^{-1} in the B3LYP and CAM-B3LYP spectra, Figure 11. For the higher-energy peaks in Figure 12, there are several molecular orbitals contributing to each dominant excitation. However, the involved orbitals generally have significant μ-oxo 2p characters. As examples, the dominant excitation around 36557 cm^{-1} has significant μ-oxo 2p → Cu 4s character while the ones near 34408 and 30110 cm^{-1} possess significant μ-oxo 2p → 2p characters, see inset of Figure 12.

CONCLUSIONS

Using cluster-model Tamm-Dancoff time-dependent DFT calculations (TDA-DFT), we have investigated the UV-Vis spectra of copper-oxo active site motifs implicated in methane to methanol conversion within the frameworks of metal-exchanged zeolites. We focused on the

CuO^+, μ-(η^2:η^2) bent-peroxo dicopper $[Cu_2O_2]^{2+}$, mono-(μ-oxo) dicopper $[Cu_2O]^{2+}$ as well as the tris-(μ-oxo) tricopper $[Cu_3O_3]^{2+}$ active site motifs. Specifically, we examined how improved agreements with experimental data can be obtained by improving the DFT density functional and by increasing the size of the cluster models used for the TDA-DFT calculations. We investigated how utilization of double-hybrid functionals would improve the calculated spectra. Lastly, for $[Cu_3O_3]^{2+}$, we examined whether TDA-DFT could provide computational evidence that this active site motif is indeed responsible for the experimental UV-Vis spectra. We found that:

1) Electron correlation (both static and dynamic) effects as well double-electron excitations are important for accurate descriptions of the excited states of CuO^+. By comparing the TDA-DFT spectra for CuO^+ against results from multi-reference wavefunction theory, we found that the best performing DFT-based methods are the double hybrids. In particular, MPW2PLYP and the long-range corrected double hybrid, ωB2PLYP, perform particularly well.
2) TDA-DFT calculations with ωB2PLYP provide very good agreements with the experimental spectra of the μ-(η^2:η^2) bent-peroxo dicopper $[Cu_2O_2]^{2+}$ and mono-(μ-oxo) dicopper $[Cu_2O]^{2+}$ active sites. For these systems, the performance of B3LYP and CAM-B3LYP improves with larger cluster sizes. However even with the largest cluster model, they still miss two signature features experimentally assigned to the $[Cu_2O_2]^{2+}$ species. The performance of ωB2PLYP also improves with cluster model size. However, with the largest cluster model, this approach predicts features that agree well with experimental assignments but are absent with B3LYP and CAM-B3LYP. For the $[Cu_2O]^{2+}$ system, B3LYP performs rather well. However, ωB2PLYP matches it for accuracy. This method yields peaks within 200 cm^{-1} of the 22700 cm^{-1} signature peak of the $[Cu_2O]^{2+}$ active site.
3) For the tricopper $[Cu_3O_3]^{2+}$ active site, we used a model cluster based on the 8MR of zeolite mordenite. This model captures the immediate first-coordination environment of the copper centers. B3LYP and CAM-B3LYP fail dramatically to reproduce the characteristic features of the experimental UV-Vis spectra. By contrast ωB2PLYP treatment of the optical spectrum of the doublet state reveals a peak at 14560 cm^{-1}, no excitations near 20000-23000 cm^{-1} and 4 bands at 25191, 30110, 34408 and 36557 cm^{-1}. These match excellently well to the features at 10000-15000, 24000, 31000, 34000 and 38500 cm^{-1} in the experimental UV-Vis spectra of

$[Cu_3O_3]^{2+}$-MOR. This is thus the first computational evidence that $[Cu_3O_3]^{2+}$ is indeed likely responsible for the empirically observed spectroscopic data.

We recommend the ωB2PLYP functional for treating the optical spectra of copper (II) oxo species that are relevant for MMC. It would be interesting to see whether ωB2PLYP can provide a rigorous description of the UV-Vis spectral changes during activation of copper-oxo sites, methane hydroxylation as well as active site regeneration.

■ ASSOCIATED CONTENT

Supporting Information.

The Supporting Information is available free of charge at https://

Optimized geometries of all systems considered in this work (PDF).

■ AUTHOR INFORMATION

Corresponding Authors

*S.O.O.: E-mail: sodoh@unr.edu

■ ACKNOWLEDGMENT

This material is based upon work supported by the National Science Foundation under Grant No. 1800387.

■ REFERENCES

(1) Göltl, F.; Michel, C.; Andrikopoulos, P. C.; Love, A. M.; Hafner, J.; Hermans, I.; Sautet, P. Computationally Exploring Confinement Effects in the Methane-to-Methanol Conversion Over Iron-Oxo Centers in Zeolites. *ACS Catal.* **2016**, *6*, 8404.

(2) Gvakharia, A.; Kort, E. A.; Brandt, A.; Peischl, J.; Ryerson, T. B.; Schwarz, J. P.; Smith, M. L.; Sweeney, C. Methane, Black Carbon, and Ethane Emissions from Natural Gas Flares in the Bakken Shale, North Dakota. *Environ. Sci. Technol.* **2017**, *51*, 5317.

(3) Kim, Y.; Kim, T. Y.; Lee, H.; Yi, J. Distinct activation of Cu-MOR for direct oxidation of methane to methanol. *Chem. Commun.* **2017**, *53*, 4116.

(4) Newton, M. A.; Knorpp, A. J.; Sushkevich, V. L.; Palagin, D.; van Bokhoven, J. A. Active sites and mechanisms in the direct conversion of methane to methanol using Cu in zeolitic hosts: a critical examination. *Chem. Soc. Rev.* **2020**, *49*, 1449.

(5) Park, M. B.; Park, E. D.; Ahn, W.-S. Recent Progress in Direct Conversion of Methane to Methanol Over Copper-Exchanged Zeolites. *Front. Chem.* **2019**, *7*, 00514.

(6) Tomkins, P.; Ranocchiari, M.; van Bokhoven, J. A. Direct Conversion of Methane to Methanol under Mild Conditions over Cu-Zeolites and beyond. *Accounts Chem. Res.* **2017**, *50*, 418.

(7) Wu, J.-F.; Gao, X.-D.; Wu, L.-M.; Wang, W. D.; Yu, S.-M.; Bai, S. Mechanistic Insights on the Direct Conversion of Methane into Methanol over Cu/Na–ZSM-5 Zeolite: Evidence from EPR and Solid-State NMR. *ACS Catal.* **2019**, *9*, 8677.

(8) Snyder, B. E. R.; Bols, M. L.; Schoonheydt, R. A.; Sels, B. F.; Solomon, E. I. Iron and Copper Active Sites in Zeolites and Their Correlation to Metalloenzymes. *Chem. Rev.* **2018**, *118*, 2718.

(9) Olsen, J. The CASSCF method: A perspective and commentary. *Int. J. Quantum Chem.* **2011**, *111*, 3267.

(10) Izsák, R. Single-reference coupled cluster methods for computing excitation energies in large molecules: The efficiency and accuracy of approximations. *WIREs Computational Molecular Science* **2020**, *10*, e1445.

(11) Runge, E.; Gross, E. K. U. Density-Functional Theory for Time-Dependent Systems. *Phys. Rev. Lett.* **1984**, *52*, 997.

(12) Casida, M. E.; Huix-Rotllant, M. In *Annual Review of Physical Chemistry, Vol 63*; Johnson, M. A., Martinez, T. J., Eds. 2012; Vol. 63, p 287.

(13) Laurent, A. D.; Jacquemin, D. TD-DFT benchmarks: A review. *Int. J. Quantum Chem.* **2013**, *113*, 2019.

(14) Maitra, N. T. Perspective: Fundamental aspects of time-dependent density functional theory. *J. Chem. Phys.* **2016**, *144*, 220901.

(15) Holland, J. P.; Green, J. C. Evaluation of Exchange-Correlation Functionals for Time-Dependent Density Functional Theory Calculations on Metal Complexes. *J. Comput. Chem.* **2010**, *31*, 1008.

(16) Latouche, C.; Skouteris, D.; Palazzetti, F.; Barone, V. TD-DFT Benchmark on Inorganic Pt(II) and Ir(III) Complexes. *J. Chem. Theory Comput.* **2015**, *11*, 3281.

(17) Petit, L.; Maldivi, P.; Adamo, C. Predictions of optical excitations in transition-metal complexes with time dependent-density functional theory: Influence of basis sets. *J. Chem. Theory Comput.* **2005**, *1*, 953.

(18) Autschbach, J. Charge-Transfer Excitations and Time-Dependent Density Functional Theory: Problems and Some Proposed Solutions. *Chemphyschem* **2009**, *10*, 1757.

(19) Dreuw, A.; Weisman, J. L.; Head-Gordon, M. Long-range charge-transfer excited states in time-dependent density functional theory require non-local exchange. *J. Chem. Phys.* **2003**, *119*, 2943.

(20) Hieringer, W.; Gorling, A. Failure of time-dependent density functional methods for excitations in spatially separated systems. *Chem. Phys. Lett.* **2006**, *419*, 557.

(21) Li, Z. D.; Liu, W. J. Spin-adapted open-shell random phase approximation and time-dependent density functional theory. I. Theory. *J. Chem. Phys.* **2010**, *133*, 064106.

(22) Li, Z. D.; Liu, W. J. Spin-adapted open-shell time-dependent density functional theory. III. An even better and simpler formulation. *J. Chem. Phys.* **2011**, *135*, 194106.

(23) Li, Z. D.; Liu, W. J.; Zhang, Y.; Suo, B. B. Spin-adapted open-shell time-dependent density functional theory. II. Theory and pilot application. *J. Chem. Phys.* **2011**, *134*, 134101.

(24) Wang, Z. K.; Li, Z. D.; Zhang, Y.; Liu, W. J. Analytic energy gradients of spin-adapted open-shell time-dependent density functional theory. *J. Chem. Phys.* **2020**, *153*, 164109.

(25) Dreuw, A.; Head-Gordon, M. Failure of Time-Dependent Density Functional Theory for Long-Range Charge-Transfer Excited States: The Zincbacteriochlorin−Bacteriochlorin and Bacteriochlorophyll−Spheroidene Complexes. *J. Am. Chem. Soc.* **2004**, *126*, 4007.

(26) Kümmel, S. Charge-Transfer Excitations: A Challenge for Time-Dependent Density Functional Theory That Has Been Met. *Adv. Energy Mater.* **2017**, *7*, 1700440.

(27) Grimme, S.; Neese, F. Double-hybrid density functional theory for excited electronic states of molecules. *J. Chem. Phys.* **2007**, *127*, 154116.

(28) Li, Z. D.; Liu, W. J. Theoretical and numerical assessments of spin-flip time-dependent density functional theory. *J. Chem. Phys.* **2012**, *136*, 024107.

(29) Shao, Y. H.; Head-Gordon, M.; Krylov, A. I. The spin-flip approach within time-dependent density functional theory: Theory and applications to diradicals. *J. Chem. Phys.* **2003**, *118*, 4807.

(30) Wang, F.; Ziegler, T. Time-dependent density functional theory based on a noncollinear formulation of the exchange-correlation potential. *J. Chem. Phys.* **2004**, *121*, 12191.

(31) Head-Gordon, M.; Rico, R. J.; Oumi, M.; Lee, T. J. A doubles correction to electronic excited states from configuration interaction in the space of single substitutions. *Chem. Phys. Lett.* **1994**, *219*, 21.

(32) Grimme, S. Semiempirical hybrid density functional with perturbative second-order correlation. *J. Chem. Phys.* **2006**, *124*, 034108.

(33) Casanova-Páez, M.; Dardis, M. B.; Goerigk, L. ωB2PLYP and ωB2GPPLYP: The First Two Double-Hybrid Density Functionals with Long-Range Correction Optimized for Excitation Energies. *J. Chem. Theory Comput.* **2019**, *15*, 4735.

(34) Woertink, J. S.; Smeets, P. J.; Groothaert, M. H.; Vance, M. A.; Sels, B. F.; Schoonheydt, R. A.; Solomon, E. I. A [Cu₂O]²⁺ core in Cu-ZSM-5, the active site in the oxidation of methane to methanol. *P. Natl. Acad. Sci. USA* **2009**, *106*, 18908.

(35) Ipek, B.; Wulfers, M. J.; Kim, H.; Göltl, F.; Hermans, I.; Smith, J. P.; Booksh, K. S.; Brown, C. M.; Lobo, R. F. Formation of $[Cu_2O_2]^{2+}$ and $[Cu_2O]^{2+}$ toward C–H Bond Activation in Cu-SSZ-13 and Cu-SSZ-39. *ACS Catal.* **2017**, *7*, 4291.

(36) Grimme, S.; Antony, J.; Ehrlich, S.; Krieg, H. A consistent and accurate ab initio parametrization of density functional dispersion correction (DFT-D) for the 94 elements H-Pu. *J. Chem. Phys.* **2010**, *132*, 154104.

(37) Grimme, S.; Ehrlich, S.; Goerigk, L. Effect of the damping function in dispersion corrected density functional theory. *J. Comput. Chem.* **2011**, *32*, 1456.

(38) Johnson, E. R.; Becke, A. D. A post-Hartree-Fock model of intermolecular interactions: Inclusion of higher-order corrections. *J. Chem. Phys.* **2006**, *124*, 174104.

(39) Hirata, S.; Head-Gordon, M. Time-dependent density functional theory within the Tamm–Dancoff approximation. *Chem. Phys. Lett.* **1999**, *314*, 291.

(40) Neese, F. The ORCA program system. *Wires Comput. Mol. Sci.* **2012**, *2*, 73.

(41) Neese, F. Software update: the ORCA program system, version 4.0. *Wires Comput. Mol. Sci.* **2018**, *8*, e1327.

(42) Becke, A. D. Density-functional exchange-energy approximation with correct asymptotic behavior. *Phys. Rev. A* **1988**, *38*, 3098.

(43) Lee, C.; Yang, W.; Parr, R. G. Development of the Colle-Salvetti correlation-energy formula into a functional of the electron density. *Phys. Rev. B.* **1988**, *37*, 785.

(44) Perdew, J. P.; Burke, K.; Ernzerhof, M. Generalized Gradient Approximation Made Simple. *Phys. Rev. Lett.* **1996**, *77*, 3865.

(45) Perdew, J. P.; Chevary, J. A.; Vosko, S. H.; Jackson, K. A.; Pederson, M. R.; Singh, D. J.; Fiolhais, C. Atoms, molecules, solids, and surfaces: Applications of the generalized gradient approximation for exchange and correlation. *Phys. Rev. B* **1992**, *46*, 6671.

(46) Zhao, Y.; Truhlar, D. G. A new local density functional for main-group thermochemistry, transition metal bonding, thermochemical kinetics, and noncovalent interactions. *J. Chem. Phys.* **2006**, *125*, 194101.

(47) Staroverov, V. N.; Scuseria, G. E.; Tao, J.; Perdew, J. P. Comparative assessment of a new nonempirical density functional: Molecules and hydrogen-bonded complexes. *J. Chem. Phys.* **2003**, *119*, 12129.

(48) Becke, A. D. Density-functional thermochemistry. III. The role of exact exchange. *J. Chem. Phys.* **1993**, *98*, 5648.

(49) Hertwig, R. H.; Koch, W. On the parameterization of the local correlation functional. What is Becke-3-LYP? *Chem. Phys. Lett.* **1997**, *268*, 345.

(50) Stephens, P. J.; Devlin, F. J.; Chabalowski, C. F.; Frisch, M. J. Ab Initio Calculation of Vibrational Absorption and Circular Dichroism Spectra Using Density Functional Force Fields. *J. Phys. Chem.* **1994**, *98*, 11623.

(51) Zhao, Y.; Truhlar, D. G. The M06 suite of density functionals for main group thermochemistry, thermochemical kinetics, noncovalent interactions, excited states, and transition elements: two new functionals and systematic testing of four M06-class functionals and 12 other functionals. *Theor. Chem. Acc.* **2008**, *120*, 215.

(52) Baker, J.; Pulay, P. Assessment of the OLYP and O3LYP density functionals for first-row transition metals. *J. Comput. Chem.* **2003**, *24*, 1184.

(53) Hoe, W.-M.; Cohen, A. J.; Handy, N. C. Assessment of a new local exchange functional OPTX. *Chem. Phys. Lett.* **2001**, *341*, 319.

(54) Adamo, C.; Barone, V. Toward reliable density functional methods without adjustable parameters: The PBE0 model. *J. Chem. Phys.* **1999**, *110*, 6158.

(55) Yanai, T.; Tew, D. P.; Handy, N. C. A new hybrid exchange–correlation functional using the Coulomb-attenuating method (CAM-B3LYP). *Chem. Phys. Lett.* **2004**, *393*, 51.

(56) Iikura, H.; Tsuneda, T.; Yanai, T.; Hirao, K. A long-range correction scheme for generalized-gradient-approximation exchange functionals. *J. Chem. Phys.* **2001**, *115*, 3540.

(57) Chai, J.-D.; Head-Gordon, M. Systematic optimization of long-range corrected hybrid density functionals. *J. Chem. Phys.* **2008**, *128*, 084106.

(58) Karton, A.; Tarnopolsky, A.; Lamère, J.-F.; Schatz, G. C.; Martin, J. M. L. Highly Accurate First-Principles Benchmark Data Sets for the Parametrization and Validation of Density Functional and Other Approximate Methods. Derivation of a Robust, Generally Applicable, Double-Hybrid Functional for Thermochemistry and Thermochemical Kinetics. *J. Phys. Chem. A* **2008**, *112*, 12868.

(59) Schwabe, T.; Grimme, S. Towards chemical accuracy for the thermodynamics of large molecules: new hybrid density functionals including non-local correlation effects. *Phys. Chem. Chem. Phys.* **2006**, *8*, 4398.

(60) Casanova-Páez, M.; Goerigk, L. Assessing the Tamm–Dancoff approximation, singlet–singlet, and singlet–triplet excitations with the latest long-range corrected double-hybrid density functionals. *J. Chem. Phys.* **2020**, *153*, 064106.

(61) Goerigk, L.; Casanova-Paez, M. The Trip to the Density Functional Theory Zoo Continues: Making a Case for Time-Dependent Double Hybrids for Excited-State Problems. *Australian Journal of Chemistry* **2020**, CH20093.

(62) Goerigk, L.; Grimme, S. Double-hybrid density functionals. *Wires Comput. Mol. Sci.* **2014**, *4*, 576.

(63) Goerigk, L.; Moellmann, J.; Grimme, S. Computation of accurate excitation energies for large organic molecules with double-hybrid density functionals. *Phys. Chem. Chem. Phys.* **2009**, *11*, 4611.

(64) Kossmann, S.; Neese, F. Efficient Structure Optimization with Second-Order Many-Body Perturbation Theory: The RIJCOSX-MP2 Method. *J. Chem. Theory Comput.* **2010**, *6*, 2325.

(65) Neese, F.; Wennmohs, F.; Hansen, A.; Becker, U. Efficient, approximate and parallel Hartree-Fock and hybrid DFT calculations. A 'chain-of-spheres' algorithm for the Hartree-Fock exchange. *Chem. Phys.* **2009**, *356*, 98.

(66) Balabanov, N. B.; Peterson, K. A. Basis set limit electronic excitation energies, ionization potentials, and electron affinities for the 3d transition metal atoms: Coupled cluster and multireference methods. *J. Chem. Phys.* **2006**, *125*, 074110.

(67) Hellweg, A.; Hättig, C.; Höfener, S.; Klopper, W. Optimized accurate auxiliary basis sets for RI-MP2 and RI-CC2 calculations for the atoms Rb to Rn. *Theor. Chem. Acc.* **2007**, *117*, 587.

(68) Aquilante, F.; Autschbach, J.; Baiardi, A.; Battaglia, S.; Borin, V. A.; Chibotaru, L. F.; Conti, I.; De Vico, L.; Delcey, M.; Galvan, I. F.; Ferre, N.; Freitag, L.; Garavelli, M.; Gong, X. J.; Knecht, S.; Larsson, E. D.; Lindh, R.; Lundberg, M.; Malmqvist, P. A.; Nenov, A.; Norell, J.; Odelius, M.; Olivucci, M.; Pedersen, T. B.; Pedraza-Gonzalez, L.; Phung, Q. M.; Pierloot, K.; Reiher, M.; Schapiro, I.; Segarra-Marti, J.*et al.* Modern quantum chemistry with Open Molcas. *J. Chem. Phys.* **2020**, *152*.

(69) Galvan, I. F.; Vacher, M.; Alavi, A.; Angeli, C.; Aquilante, F.; Autschbach, J.; Bao, J. J.; Bokarev, S. I.; Bogdanov, N. A.; Carlson, R. K.; Chibotaru, L. F.; Creutzberg, J.; Dattani, N.; Delcey, M. G.; Dong, S. J. S.; Dreuw, A.; Freitag, L.; Frutos, L. M.; Gagliardi, L.; Gendron, F.; Giussani, A.; Gonzalez, L.; Grell, G.; Guo, M. Y.; Hoyer, C. E.; Johansson, M.; Keller, S.; Knecht, S.; Kovacevic, G.; Kallman, E.*et al.* OpenMolcas: From Source Code to Insight. *J. Chem. Theory Comput.* **2019**, *15*, 5925.

(70) Kulkarni, A. R.; Zhao, Z.-J.; Siahrostami, S.; Nørskov, J. K.; Studt, F. Monocopper Active Site for Partial Methane Oxidation in Cu-Exchanged 8MR Zeolites. *ACS Catal.* **2016**, *6*, 6531.

(71) Roos, B. O.; Lindh, R.; Malmqvist, P. A.; Veryazov, V.; Widmark, P. O. Main group atoms and dimers studied with a new relativistic ANO basis set. *J. Phys. Chem. A* **2004**, *108*, 2851.

(72) Roos, B. O.; Lindh, R.; Malmqvist, P. A.; Veryazov, V.; Widmark, P. O. New relativistic ANO basis sets for transition metal atoms. *J. Phys. Chem. A* **2005**, *109*, 6575.

(73) Reiher, M. Relativistic Douglas–Kroll–Hess theory. *WIREs Computational Molecular Science* **2012**, *2*, 139.

(74) Zobel, J. P.; Nogueira, J. J.; Gonzalez, L. The IPEA dilemma in CASPT2. *Chem. Sci.* **2017**, *8*, 1482.

(75) Forsberg, N.; Malmqvist, P.-Å. Multiconfiguration perturbation theory with imaginary level shift. *Chem. Phys. Lett.* **1997**, *274*, 196.

(76) Srnec, M.; Navrátil, R.; Andris, E.; Jašík, J.; Roithová, J. Experimentally Calibrated Analysis of the Electronic Structure of CuO+: Implications for Reactivity. *Angew. Chem. Int. Edit.* **2018**, *57*, 17053.

(77) Vanelderen, P.; Snyder, B. E. R.; Tsai, M.-L.; Hadt, R. G.; Vancauwenbergh, J.; Coussens, O.; Schoonheydt, R. A.; Sels, B. F.; Solomon, E. I. Spectroscopic Definition of the Copper Active Sites in Mordenite: Selective Methane Oxidation. *J. Am. Chem. Soc.* **2015**, *137*, 6383.

(78) Dandu, N. K.; Adeyiga, O.; Panthi, D.; Bird, S. A.; Odoh, S. O. Performance of density functional theory for describing hetero-metallic active-site motifs for methane-to-methanol conversion in metal-exchanged zeolites. *J. Comput. Chem.* **2018**, *39*, 2667.

(79) Dandu, N. K.; Reed, J. A.; Odoh, S. O. Performance of Density Functional Theory for Predicting Methane-to-Methanol Conversion by a Tri-Copper Complex. *J. Phys. Chem. C* **2018**, *122*, 1024.

(80) Vogiatzis, K. D.; Li, G.; Hensen, E. J. M.; Gagliardi, L.; Pidko, E. A. Electronic Structure of the $[Cu_3(\mu\text{-}O)_3]^{2+}$ Cluster in Mordenite Zeolite and Its Effects on the Methane to Methanol Oxidation. *J. Phys. Chem. C* **2017**, *121*, 22295.

(81) Grundner, S.; Markovits, M. A. C.; Li, G.; Tromp, M.; Pidko, E. A.; Hensen, E. J. M.; Jentys, A.; Sanchez-Sanchez, M.; Lercher, J. A. Single-site trinuclear copper oxygen clusters in mordenite for selective conversion of methane to methanol. *Nat. Commun.* **2015**, *6*, 7546.

(82) Ikuno, T.; Grundner, S.; Jentys, A.; Li, G.; Pidko, E.; Fulton, J.; Sanchez-Sanchez, M.; Lercher, J. A. Formation of Active Cu-oxo Clusters for Methane Oxidation in Cu-Exchanged Mordenite. *J. Phys. Chem. C* **2019**, *123*, 8759.

For Table of Contents Only

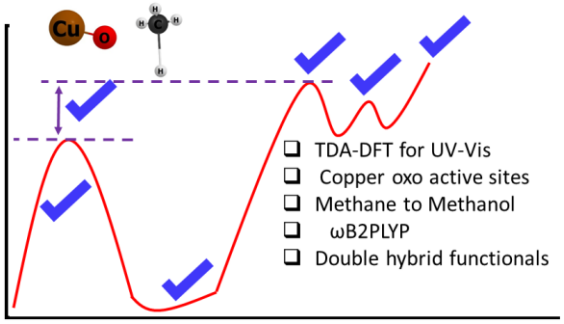

Synopsis: Copper-exchanged zeolites are useful for converting methane to methanol. The active Cu_xO_y sites are often characterized with UV-Vis spectroscopy. However, the optical spectra of these species are often problematic to calculate with Tamm-Dancoff time-dependent density functional theory, TDA-DFT. Double-hybrid density functionals rectify many of these issues. ωB2PLYP provides accurate results for CuO^+, μ-(η^2:η^2) bent-peroxo dicopper $[Cu_2O_2]^{2+}$, and mono-(μ-oxo) dicopper $[Cu_2O]^{2+}$. We provide computational evidence for the UV-Vis spectra of the tris-(μ-oxo) tricopper $[Cu_3O_3]^{2+}$ active site.